Post-print version of the paper by Janakiram et al. in ACS Applied Materials & Interfaces 2019, 11, 33302−33313. https://doi.org/10.1021/acsami.9b09920

Manipulation of Fibril Surfaces in Nanocellulose-based Hybrid Facilitated Transport Membranes for Enhanced CO_2 Capture

*Saravanan Janakiram[1], Xinyi Yu[1], Luca Ansaloni[2], Zhongde Dai[1], Liyuan Deng[1]**

[1]Department of Chemical Engineering, Norwegian University of Science and Technology (NTNU), Trondheim, NO-7491, Norway

[2]Department of Sustainable Energy Technology, SINTEF Industry, 0373 Oslo, Norway

*corresponding author: liyuan.deng@ntnu.no

Keywords

Nanocellulose; facilitated transport; CO_2 Capture; surface modification; biomaterial

Abstract

The transition towards sustainable processing entails the use of bio-based alternatives as functional materials to reduce overall carbon footprint. Nanocellulose, due to its natural availability, biodegradability, excellent mechanical properties, tunable surface, and high aspect ratio, is attracting more and more interests as nanoscale additive in polymeric membranes. In this work, an effective way to modify nanocellulose fibril surfaces for performance enhancement in CO_2 separation membranes has been demonstrated. The functionalization promptly triggered intrinsic property responses in favour of nanofiber dispersion and CO_2 transport. Thin composite membranes containing the modified nanofibers in water-swelling polyvinyl alcohol (PVA) as well as in the blend of sterically-hindered polyallylamine (SHPAA) and PVA were fabricated and tested using humid gas permeation tests. Defect-free ultrathin (300 nm) hybrid selective layers containing evenly distributed nanofibers were successfully coated. The addition of nanocellulose exhibited enhanced CO_2 permeance and CO_2/N_2 selectivity compared to the neat PVA membranes; CO_2 permeance up to 652 GPU with a CO_2/N_2 selectivity of 41.3 were documented. Functionalization plays a categorical role in the dispersion of nanocellulose fibrils in the SHPAA/PVA blend, increasing the steric stabilization and interface compatibility with the polymer matrix. The tuned interface with PEG groups act as sites for water clusters retention and increased CO_2 solubility, thus creating fast diffusion pathways for CO_2 transport.

1. Introduction

Nanocellulose largely constitute an interesting class of natural nanomaterials that are derived from the crystalline cellulosic domains of biomass[1]. Primarily because of the bio-based origin and ability to be functionalized due to the presence of a large number of hydroxyl groups, nanocellulose is of increasing interest for the synthesis of novel functional materials [2,3]. In recent years, nanocellulose, both as nanocrystals (CNC) or nanowhiskers (CNW) and as microfibrillated cellulose (MFC), is used as an engineering material in a wide range of products ranging from packaging industries to medical applications [4,5]. Particularly, nanocellulose fibrils are being used as a structural additive in various other chemicals to produce novel products[6,7]. The motivation behind such usage is attributed to the reduction of environmental impacts and carbon footprint in the production process since nanocellulose can be classified as renewable polymer.

Although cellulose acetate has been commercially used in gas separation membranes for decades, in recent times, nanocellulose has been increasingly studied as additives in polymeric gas separation membranes[8]. As a 1D material with a high aspect ratio and semi-crystalline nature due to H-bonding capacity, nanocellulose enhances the mechanical properties of membranes [8]. While their long lateral dimension impels effective disruption of polymer chain packing along the length, their negligible thicknesses (diameter) hardly affects the overall selective layer thickness. Thus, the nanoscale property changes arising due to filler addition help in enhancing both transport properties and durability of the membrane[9] Additionally, their affinity towards CO_2 and high hydrophilicity can also be leveraged to function as enhancement additives in membranes for CO_2 capture. Ansaloni et al. [10] reported the use of nanocellulose fibrils in Lupamin (PVAm) matrix with an increased separation performance of both CO_2/N_2 and CO_2/CH_4 gas pairs. At high humidity, Lupamin contributes to the facilitated transport of CO_2 while the intrinsic separation ability of nanocellulose could not be efficiently utilized. Venturi et al. [11] further established a relationship between permeability and relative humidity in terms of water solubility modeled using the Park model [12]. The promising composite containing 30% MFC in Lupamin exhibited a performance of CO_2 permeability around 90 Barrer with a selectivity of 218 and 184 for CO_2/N_2 and CO_2/CH_4, respectively.

While nanocellulose has been added to polymers in membrane applications for other separation applications [13–15], their application in CO_2 capture membranes is still not widely investigated. Since selective layer thickness of less than 500 nm is usually preferred for an attractive CO_2

capture membrane[16], as a 1D material with sub-50 nm diameter, their potential as nanofillers in these ultrathin layers is noteworthy. However, a recurring analogy of challenges when using nanocellulose in hybrid membranes and their application as reinforcements in composites is the complexity over the control of the polymer/nanocellulose interface. The surface chemistry of nanocellulose fibrils determines the establishment of the interface morphology and depends on the process of synthesis, which is the isolation of nanocellulose from native fibrils by chemical, mechanical or enzymatic methods. An ideal interface (i.e., perfect adhesion between the polymer phase and the fibrils[17] is generally preferred for better exploitation of filler's properties in composites. Surface chemistry plays a major role in determining the properties of the filler-polymer interface, and efficient surface modification acts as a tool to tailor these properties [18]. In CO_2 capture membranes, fillers' functionalization has been found to influence both the morphology and transport properties of hybrid membranes. Although functionalization is a well-explored strategy for efficient use of nanocellulose in different applications[19–21], functionalization of nanomaterials in CO_2 capture membranes has been widely limited to Carbon nanotubes (CNTs) , Graphene oxide(GO nanosheets), Polyhedral Oligomeric Silsesquioxanes (POSS) and Metal Oxide Frameworks (MOFs) [8,22]. Shen et al. [23] functionalized GO nanosheets with PEI prior to incorporation in PVAm matrix, increasing both CO_2 permeance and CO_2/N_2 selectivity. The PEI groups contributed to increased stability of nanofillers in the polymer matrix. Li et al. [24] increased both diffusivity selectivity and solubility selectivity by functionalizing GO with PEG and PEI functional moieties and using the functionalized fillers in Pebax matrix. In a study by Ansaloni et al. [25], amine functionalization of CNTs was found to increase the compatibility of Multiwalled CNTs in PVAm matrix thus helping to achieve long-term reliable high-pressure separation performance. In most cases, the functional moieties are chosen to improve dispersibility and other CO_2-philic properties and to simultaneously strengthen the polymer matrix and aid CO_2 transport.

The current work focuses on the use of nanocellulose in facilitated transport membranes and the effects of the nancellulose addition on the gas transport through the membranes. A facile surface modification procedure to introduce functional moieties of varying properties was developed as a "one-pot" process to manipulate the nanocellulose surface. The role of functionalized surfaces in hybrid membranes has been systematically investigated using various filler-phase characterization techniques like TGA, XRD and water uptake tests. Given that the industrial realization of hybrid membranes requires ultrathin coating of selective layer on a porous polymeric support to enhance the transmembrane flux [16], composite membranes

containing functionalized fillers with selective layer thicknesses less than 300 nm were successfully fabricated and tested. The high aspect ratio of the nanocellulose fibrils enabled spatial distribution of fibres along the surface leading to ultrathin defect-free selective layers. The influence of modified fillers on the morphology of hybrid membranes with different polymer matrices and their corresponding gas permeation properties have been systematically investigated. To the best of our knowledge, the present study is the first to investigate the influences of surface properties of nanocellulose-based 1D nanofillers when used in facilitated transport polymers from fabrication until application in CO_2 capture.

2. Materials and methods

2.1. Materials

Poly(allylamine hydrochloride) (Mw=120,000-200,000) was purchased from Thermo Fisher Scientific, Sweden and was purified and modified prior to use. Potassium hydroxide (pellets, 85%-100%), polyvinylalcohol (Mw=89,000-98,000, 89% hydrolyzed), 1-Ethyl-3-(3-dimethylaminopropyl) carbodiimide, N-hydroxysulfosuccinimide, 2-bromopropane, Methanol (anhydrous, >99.8), 4arm-poly(ethylene glycol)-NH_2 (Mn=5,000), 8arm-poly(ethylene glycol)-NH_2 (hexaglycerol core, Mn=10,000), Trimethylolpropane tris[poly(propylene glycol), amine terminated] ether (Mw=1368), β-Alanine (99%), 1-(2-Aminoethyl) piperazine (99%) and Sarcosine (98%) were used as received from Sigma-Aldrich, Norway. Microfibrillated cellulose (MFC, originated from eucalyptus pulp) and sodium carboxymethylated cellulose (CMC, Na^+ content *2830 µmol/g*) were provided by INOFIB, France, as suspensions in water with a solid content of 3.3 and 1.7 wt%, respectively. Polyvinylidene fluoride (PVDF) Ultrafiltration membrane (50k MW) with polypropylene (PP) substrate was provided by Synder Filtration, USA. 3M™ Fluorinert™ Electronic Liquid FC-72 was used as received from Kemi-Intressen, Sweden. The gases used in the gas permeation tests included a CO_2/N_2 mixture (10 vol.% CO_2 in N_2) and CH_4 (99.95%) were purchased from AGA, Norway and used as received.

Synthesis of sterically hindered polyallylamine (SHPAA)

Purified polyallylamine is obtained by the reaction of poly(allylamine hydrochloride) with equivalent KOH in the methanol at room temperature for 48h. The precipitated salt is removed by centrifugation followed by filtration to obtain a clear solution of PAA in methanol. The solution is then dried in a ventilated oven at 60 °C to obtain dry polymer if needed. In order to

sterically hinder the primary amines present in the backbone chain of PAA, PAA solution in methanol is treated with one equivalent of 2-bromopropane with a stoichiometric equivalent of KOH by refluxing at 50 °C for 48h as reported by Zhao and Ho [26]. Similar purification procedure was adopted to result in a dry polymer which is then stored in a desiccator to prevent adsorption of water. Successful modification of PAA to SHPAA was confirmed by FTIR spectrum that is in agreement with the literature [26].

Modification of nanocellulose fibrils

Carboxymethylation is a process that imparts negative charges on the surface of nanocellulose to increase the electrostatic stability of the nanofibrils in dispersions [4]. The carboxymethylated nanocellulose (CMC) used in this study was provided by Inofib SAS as a 3.7 wt% dispersion in water. Modification of MFC surfaces by grafting of different moieties was achieved by EDC/NHS activation reaction, where EDC represents 1-Ethyl-3-(3-dimethylaminopropyl) carbodiimide, and NHS is N-hydroxysulfosuccinimide.

EDC/NHS coupling is particularly advantageous due to the use of aqueous medium thus avoiding hazardous reagents. Retention of fibers in aqueous dispersion is required to avoid aggregation, thereby preserving the 1D nano-morphology, and for compatibility when added to aqueous polymer solutions. Additionally, with the availability of CMC, the carboxyl groups in the fibril surface are directly available for coupling with the amine-containing reactants through a simple mechanism as described in **Scheme 1**. The versatility of this methodology to graft numerous small molecules with primary amine groups is also noteworthy. To activate the carboxyl groups, 750 mg of EDC and 500 mg of NHS was added to 100 g of 2 mg/g CMC dispersion and the solution was stirred for 30 mins. The large amount of catalyst EDC was used to compensate for possibilities of deactivation due to the presence of impurities arising from the cellulose fibrillation process. The activated dispersion was used for grafting with different chemicals. Hence, the number of sites available for grafting was assumed to be the same in each case. The reactive component containing a primary amine was then added in stoichiometric quantities to the activated dispersion and the reaction was left to proceed at room temperature for 24h. Three polymeric variants and one amino acid-based reactants were chosen for grafting as seen in **Figure 1**. After the reaction, the products were separated by centrifugation into gel-like precipitates with similar solid contents. The centrifugation was repeated by rinsing with DI water until the supernatant was clear of EDC and the reactants

were added by verification using FTIR to ensure that no free reactants were present in the final product.

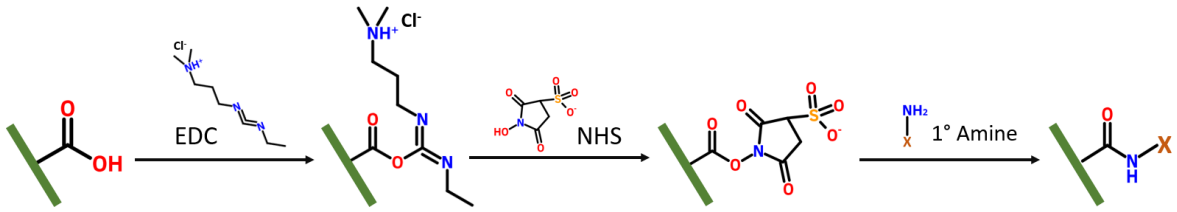

Scheme 1: EDC/NHS Chemistry of coupling carboxylic group with primary amine to form a stable amide linkage.

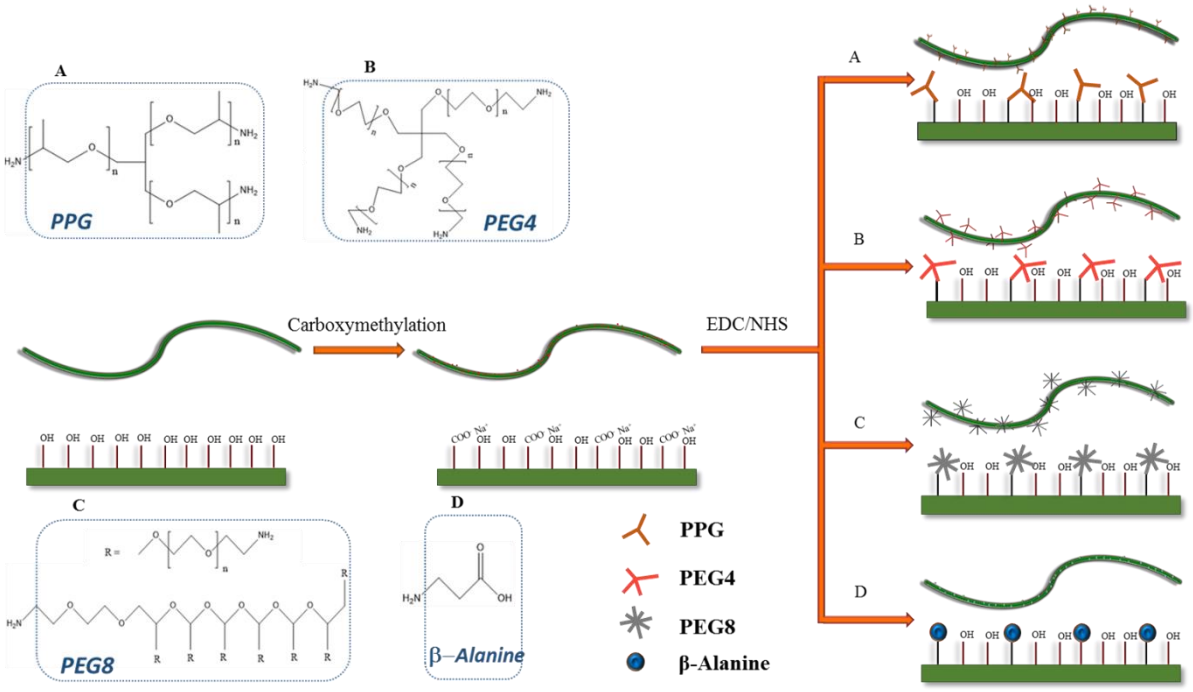

Figure 1. Nanocellulose fibril surface modification performed in this study.

2.2. Fabrication of composite membranes

PVA pellets are dissolved in water at 80 °C in reflux conditions to obtain 4 wt% solution. The solution of PAA or SHPAA in water is obtained by stirring a known amount of dry polymer in the required amount of water for 24h at room temperature. The cast solution used for thin film coatings was 2.5 wt% polymer in case of PVA and 1-2 wt% polymer in case of SHPAA/PVA blends. The blend ratio was 90% SHPAA and 10% PVA to make use of the excellent film forming abilities of PVA. The mobile carrier was synthesized by reaction of equimolar 1-(2-

Aminoethyl) piperazine with Sarcosine in water for 24h at room temperature. The chosen concentration of mobile carriers was 40 wt% of the total polymer content in the casting solution.

In the case of cast solution for the hybrid selective layer, nanocellulose fibrils were considered as additives and hence the ratios were taken as the ratio of total polymer phase. For example, 10% MFC in PVA solution contained 10% MFC and 90% PVA in water with total solids of 2.5 wt%.

The thin composite materials were fabricated by bar coating technique on PVDF ultrafiltration support. The supports were treated at 45 °C in running tap water for 1 h followed by rinsing in DI water at room temperature for 30 min to remove the pore-protection chemicals. After coating, the membranes are dried in a vacuum oven at 60 °C for 2 h to remove residual solvent. The thin composite membranes were used for gas permeation tests. For characterizations in XPS, FTIR, TGA, and water sorption tests, dense bulk films of functionalized nanofillers were made by solvent evaporation of casting solution on Teflon dish.

2.3. Membrane characterization

SEM

The morphological analysis for membrane surfaces and cross sections were performed by a TM3030 table top scanning electron microscope (SEM, Hitachi High Technologies America, Inc.). Cross sections were obtained by fracturing membrane samples into liquid nitrogen. In order to get conductive surfaces, all the samples were coated by gold in Argon atmosphere for 1 min before SEM analysis. Secondary electron and backscattered electron beams with the intensity of 15kV were used as mixed electron signal.

High-resolution SEM for determining thicknesses were carried out using Field Emission SEM APREO (FEI, Thermo Fisher Scientific, USA) using in lens detector in Immersion mode. The samples were coated with 4nm Pd/Pt alloy prior to measurement.

S(T)EM

Structural characterization of the nanoparticles was analyzed by Hitachi S-5500 S(T)EM (Hitachi High Technologies America, Inc.). S-5500 is an in-lens cold field emission electron microscope using secondary and low/high-angle backscattered electrons with achievable resolution down to 0.4 nm. Bright field and dark field detectors were used for transmission

measurements. STEM samples were prepared by dropping ultra-dilute nanoparticle suspension (0.1 wt%) on 300 mesh Cu grids (Electron Microscopy Sciences, FCF300-Cu).

Water uptake

A pressure decay apparatus was used to measure the water uptake of different dense nanocellulose films at 35 °C. A description of the setup is reported elsewhere [27].A small test piece of dry sample was initially held at vacuum in an isolated volume (35.1 ± 0.2 cm^3). Water at necessary activity was stabilized in a pre-chamber volume (49.7 ± 0.2 cm^3) whose pressure was closely monitored with a precision pressure sensor (full scale of 100 mbar 121A, MKS Instrument, USA). Once the conditions in the pre-chamber are stable, the two chambers are connected (by opening a valve) and the pressure decline to the equilibrium value is noted. The drop in pressure in the calibrated volume is associated with with the water uptake of the sample (g/g_{pol}) at that particular water activity [10,28,29]. The procedure is repeated in progressive steps, increasing the water vapor pressure surrounding the sample. Multiple samples were tested in order to ensure the tests repeatability.

Thermal properties

The dense films of different nanocellulose were analysed in thermogravimetric analyser (TGA, TG 209 F1 Libra , Netzsch, Germany). 5 mg of the samples were loaded onto a sample holder and heated from room temperature to up to 800 °C at a constant rate of 20 K min^{-1} under N_2 atmosphere (purge rate 60 ml min^{-1}). The mass change was recorded for each sample as a function of temperature.

FTIR

The dense films of functionalized nanocellulose were analysed with Thermo Nicolet Nexus spectrometer (smart endurance reflection cell in attenuated total reflectance (ATR) mode with a diamond crystal) for the Fourier-transform infrared (FTIR) spectroscopy. The spectra were built on the average of 16 scans with a resolution of 4 cm^{-1} wavenumber between the wavenumbers of 4000 cm^{-1} to 800 cm^{-1}.

XRD

Bruker D8 A25 DaVinci X-ray Diffractometer (Bruker Corporation, USA) was used to analyze the crystallinity and phase structures of samples (with CuKα radiation, LynxEye™ SuperSpeed detector). The diffraction signal was collected at the range of $5° < 2\theta < 75°$ during the test with a scanning speed of 0.044 °/step. Square film samples (1 cm × 1 cm) were tiled on a Si wafer

sample holder and fixed with vacuum grease. The influences on the crystallinity of cellulose-based nanoparticles after EDC functionalization were compared by analyzing XRD spectra between pure nanocellulose and other functionalized nanocellulose types. All the tests were carried out with dry dense films and performed at room temperature and indoor humidity.

AFM

The topographic analysis was carried out using an Atomic Force Microscope (AFM), Veeco diMultimode V (Veeco Instruments, Inc., USA). A silicon nitride tip was employed in a Scan Asyst QNM tapping mode. The samples were prepared on Mica sheets by drying a drop of casting solution and drying under similar conditions to that of the membrane.

2.4. Mixed gas permeation

The CO_2 separation performance of the fabricated hybrid membranes was measured by a mixed gas permeation rig with controlled humidity similar to our previous studies[30]. The feed side had a flow of 200 ml min^{-1} of 90/10 v/v CO_2/N_2 mixture at an upstream pressure of 1.7 bar. The sweep gas consisted of CH_4 flowing at a rate of 100 ml min^{-1} at a pressure of 1.05 bar. Both feed and the sweep streams are bubbled through a tank containing water to get saturated gas streams. A gas chromatograph (490 Micro GC, Agilent) calibrated at the range of operation was used to analyse the real-time composition of retentate, permeate and feed streams periodically. The permeance of the *i*-th component was calculated using the following equation:

$$P_i = \frac{V_p(1-y_{H_2O})y_i}{((p_{i,f}-p_{i,r})-p_{i,p})A} \quad (1)$$

Where V_p is the total permeate flow (ml/s) measured using a bubble flow meter at steady state conditions. y_{H_2O} and y_i are the molar fraction of the water and permeating species in the permeate flow respectively. $p_{i,f}$, $p_{i,r}$ and $p_{i,p}$ are the partial pressures ($cmHg^{-1}$) of the *i*-th species in the feed, retentate and permeate, respectively. A is the permeation area (cm^2). The permeance is reported in GPU (1 GPU = 10^{-6} cm^3(STP) cm^{-2} s^{-1} $cmHg^{-1}$ = 3.35 x 10^{-10} mol m^{-2} s^{-1} Pa^{-1}) By using gaseous mixture, it was also possible to calculate the separation factor, as given in Equation 2:

$$\alpha_{i/j} = \frac{y_i/x_i}{y_j/x_j} \quad (2)$$

In order to provide a proper description of the permeance values, the stage cut was always kept below 5% for all the experiments.

3. Results and discussion

3.1. Characterization of nanocellulose

Chemical interactions due to functionalization of the MFC fibril surface with polymeric moieties are determined by FTIR spectroscopy of the dry films. The spectra of various modified fillers in comparison with native MFC fibrils are shown in **Figure 2**. Typical absorption peaks of the nanocellulose structure are the C-O-C stretching (1060 cm^{-1}), the C-H symmetrical stretching (2800 cm^{-1}) and the broad peak associated with -OH stretching in polymeric hydrogen bonding (~ 3200-3500 cm^{-1}). The characteristic strong broad peak at 1605 cm^{-1} confirms the presence COO^- groups in the CMC (stretching in sodium form [31]). Additionally, there is reduced intensity of –OH stretching which indicates partial substitution of surface hydroxyl groups by –COO- groups.

Successful functionalization of MFC using carbodiimide-catalyzed reaction (MFC-PPG) is also confirmed by the FTIR spectra. The peak at 1097 cm^{-1} can be attributed to the antisymmetric C-O-C stretching of the PPG moiety in addition to the C-O-C groups present in the cellulose. Large amounts of methyl groups are marked as peaks at around 2865 cm^{-1}, 1453 cm^{-1} and 1342 cm^{-1} due to both C-H stretching and C-H bending. The intensity of bending vibrations at ~ 2850 cm^{-1} is more pronounced in the case of PPG- and PEG-functionalized nanofillers while, in other cases, this is inherited from the cellulosic backbone. Very few differences in the spectra were observed between the PEG-functionalized systems owing to their close resemblance in chemical structure. The broad peak on the spectrum of β-Alanine (MFC-β-Alanine) between 3200 cm^{-1} to 2300 cm^{-1} consists of the band of O-H stretching on carboxylic acid, overlapping with the peaks of C-H stretching and N-H stretching.

It can be concluded that all the functional moieties successfully reacted with CMC because of the formation of an amide bond (NH deformation at 1530 cm^{-1} and C=O stretching of secondary amine at 1643 cm^{-1}) in the spectra of all modified celluloses [32]. No obvious peaks corresponding to other components can be found in the spectra, meaning that unused reactants and catalysts have been effectively washed out. Free COO^- groups can still be observed from the small

characteristic shoulder of C=O at 1605 cm^{-1}, which is possibly related to the incomplete conversion limited by the availability of reactants containing the functional groups.

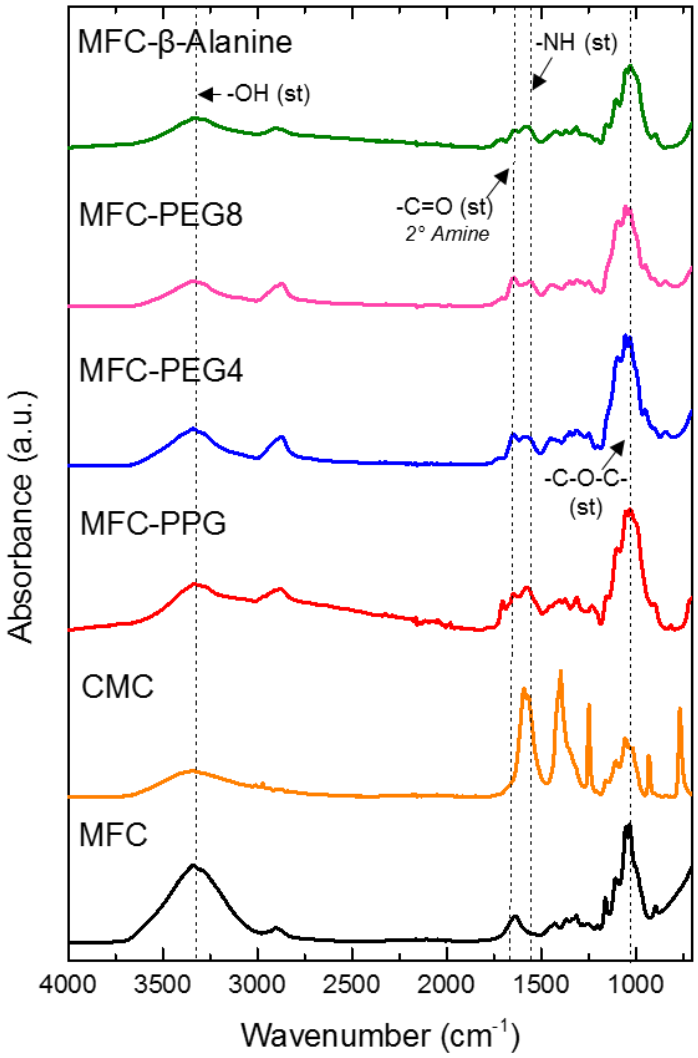

Figure 2. FTIR Spectra of various nanofillers.

Both native nanocellulose (MFC) and functionalized-nanocellulose fibrils (MFC-PEG4) are seen as fibrous bundles in S(T)EM images shown in **Figure 3**. Only MFC-PEG4 was shown as representative for functionalized fibrils owing to the similarity of all functionalized-nanocellulose fibrils; All the individual fibers were a few hundred nanometers long with diameters less than 50 nm, revealing their characteristic 1D structure [8]. A classical web-like network of fibril clusters can be seen with entangled filaments of cellulose as observed in the typical TEM analysis of cellulose nanofibrils in literature [8,33]. H-bonding capacity is believed to be increased with the functionalized fibrils, leading to densification of the matrix while

drying in the copper grid, as clearly seen in **Figure 3**. The fibril morphology is preserved despite the functionalization of moieties, which shows corroborating existence through a stable dispersion with negligible agglomeration at the fibril level.

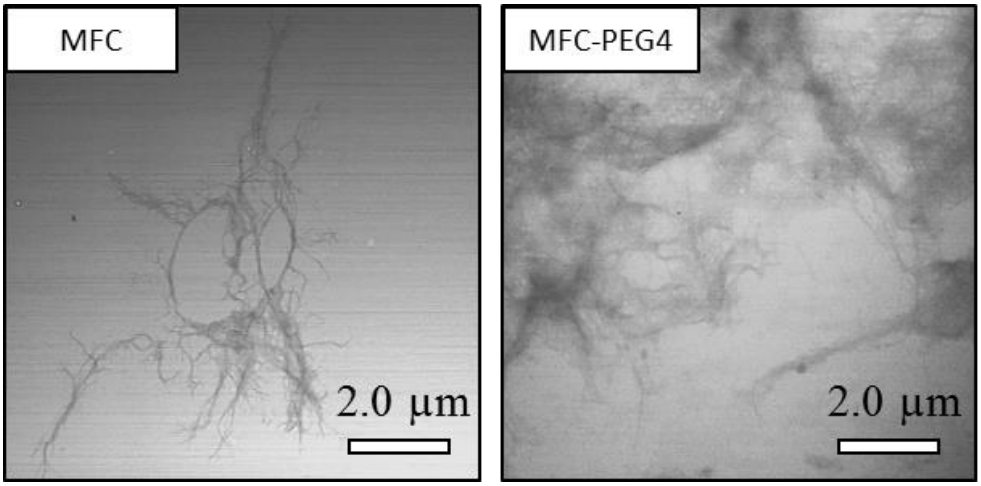

Figure 3. STEM imaging of unmodified (MFC) and modified (PEG4-MFC) nanocellulose fibrils.

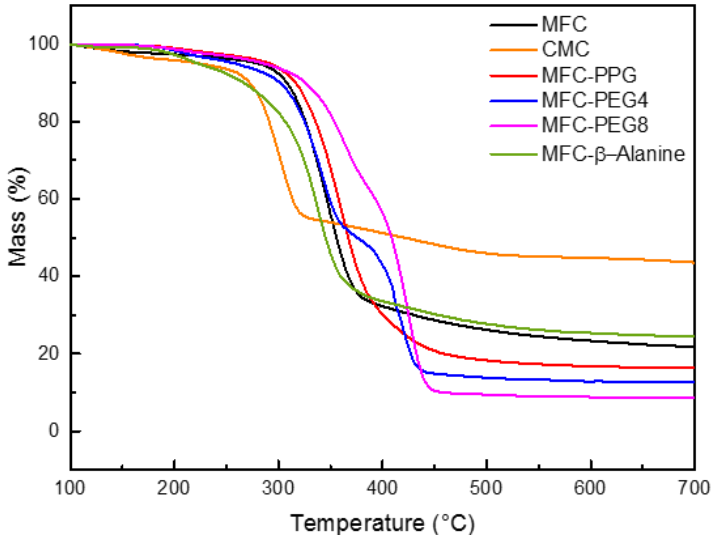

Figure 4. TGA of modified and unmodified nanofibrils

Thermal properties of the films of native and functionalized MFC are analysed by TGA and the mass loss profiles are shown in **Figure 4**. The process of functionalization induces marked differences in the onset degradation temperature of the fillers with CMC beginning as early as

273 °C. This is due to the effect of lower ionic bond strength which leads to rapid decarboxylation. In contrast, the accompanying residual mass was 43% of the initial weight. This change in weight may be attributed to the carbonized material and inorganic sodium salt used to stabilize anionic charges. Compared to the other functionalized celluloses, MFC-PEG8 showed the best tolerance towards degradation, possibly due to the higher molecular weight of the grafted polymer. MFC-PEG8 exhibited the highest onset at 327 °C and end set at 447 °C. Additionally, the residual mass decreases with increasing molecular weight of the grafted component, due to the lower amounts of pyrolyzed solid residue, which is sourced mainly from cellulosic material[34]. In general, nanocellulose fibrils functionalized with polymer moieties are found to have higher onset temperatures than those of the MFC with β-Alanine and CMC. Additionally, CMC and β-Alanine are also found to exhibit considerable mass loss at relatively lower temperatures when compared to other fillers. Both MFC-PEG4 and MFC-PEG8 are seen to have two inflection points exhibiting a second onset temperature at 393 °C and 399 °C, respectively. This can be attributed to the fact that the amide bond ruptures at relatively lower energy (C-N bond energy = 305 kJ/mol) while a large amount of ethylene oxide (EO) groups present in the polymer backbone disrupt after that (C-O bond energy = 358 kJ/mol). The amide bond formation using EDC chemistry can be considered as a powerful tool for functionalization since the bond disruption happens only at high temperature. Additionally, sensitive thermal profiles also give further proof to the occurrence of functionalization.

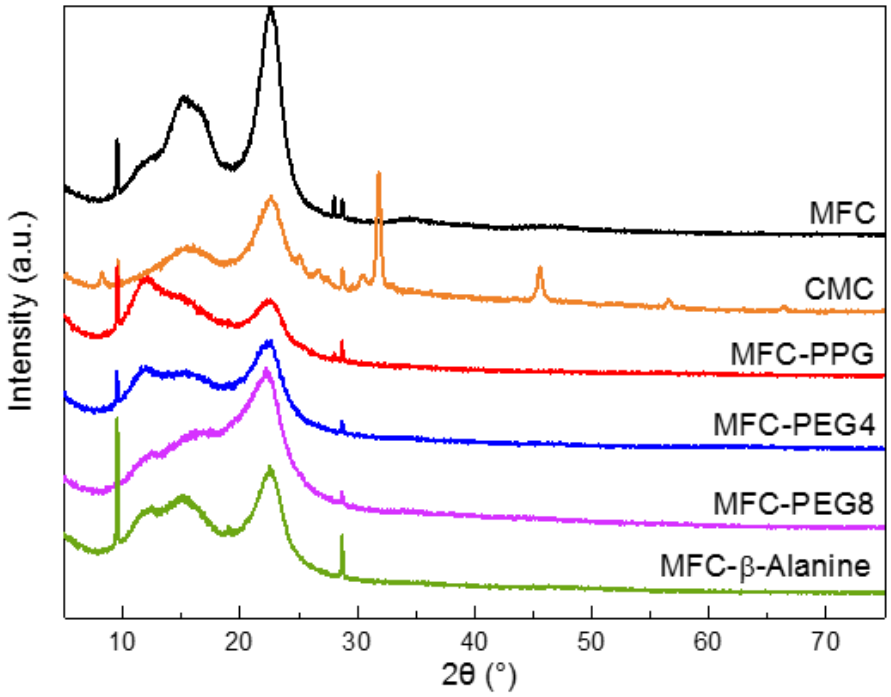

Figure 5. XRD pattern of modified and unmodified nanocellulose fibrils

The crystal structure of the modified nanocellulose films was studied by X-Ray diffraction of the films made of fillers as shown in **Figure 5**. Two types of crystalline forms of cellulose, cellulose I (parallel chains) and cellulose II (anti-parallel chains) have been found in the samples, reflecting characteristic peaks on the XRD spectrum at different positions [35]. These conformations of cellulose depends on the nature of intramolecular and intermolecular hydrogen bonding formation. Usually, the crystalline region and the amorphous region both co-exist in the microstructure of nanocellulose. The crystalline index (CI) of samples are estimated by Segal's method without normalizing the original data [35]:

$$X_c = \frac{I_{002} - I_{am}}{I_{002}} \times 100$$

where X_c is the crystallinity degree of samples, I_{002} is the maximum intensity taken at 002 peak where around 2θ = 22.8 °, I_{am} is the minimum intensity of between 18° and 20° which is due to the amorphous part of cellulose. This method was used to calculate the ratio of the intensity of crystalline peak to the total intensity. The calculated X_c is summarized in **Table 1.**

Table 1. The characteristic peaks and crystallinity index of nanocellulose and functionalized nanocellulose.

Filler	2θ (°)	Miller indices	I_{002} (a.u.)	I_{am} (a.u.)	CI (%)
MFC	12.4	-110 (cellulose II)	15.07	4.52	70.0
	15.1	-110 (cellulose I)			
	16.6	110 (cellulose I)			
	22.5	200			
CMC	15.7	110 (cellulose I)	7.96	3.57	55.1
	22.6	200			
MFC-PPG	11.9	-110 (cellulose II)	5.26	3.41	35.2
	15.3	-110 (cellulose I)			
	22.6	200			
MFC-PEG4	11.9	-110 (cellulose II)	7.38	4.23	42.6
	15.3	-110 (cellulose I)			
	22.5	200			
MFC-PEG8	12.3	-110 (cellulose II)	10.82	6.41	40.7
	15.8	-110 (cellulose I)			

	22.3	200			
MFC-β-Alanine	12.3	-110 (cellulose II)	8.55	4.04	52.7
	15.1	-110 (cellulose I)			
	22.6	200			

Both MFC and CMC show typical peaks of cellulose structure at 22.6^0 and 15.6^0 while the sharp peaks at 31.8^0 and 45.5^0 in the CMC spectrum correspond to inorganic content constituting the sodium salts [36,37]. The sharp prominent peak of the 002 plane, characteristic of pure MFC, is found to be notably influenced by functionalization. Small molecules (CMC and β-Alanine) are found to elicit no obvious shifts in the peaks; therefore, they present only small changes in the crystal structure. Nevertheless, both result in about 20% reduction in crystallinity compared to MFC. MFCs that have been modified with high MW polymers display broader and indistinct peaks, indicating the formation of smaller crystal sizes. A slight shift towards lower angles is observed for the 002 peak as the MW of the bonded polymer is increased, suggesting increased d-spacing [38]. Although linear PEG has been reported to have high crystallinity (especially for high MW [39]), the MFC-PEG8 sample obtained in this work showed slightly lower crystallinity than MFC-PEG4. This is possibly because the highly branched structure intrudes to the cellulose lattice planes disrupting the crystallinity due to hydrogen bonding. In general, the functionalized MFCs are found to be characterized by lower crystallinity when compared with the pristine nanocellulose fibrils. Although the hydrogen bonding capacity of nanocellulose fibrils facilitates formation of films, the high crystallinity often leads to increased brittleness in the films. Thus, through functionalization, the reduced crystallinity also helped in the fabrication of softer nanocellulose films. Furthermore, the reduced overall crystallinity is a positive asset to both gas permeation (crystalline domains are assumed to be impermeable to gases) and mechanical flexibility (easier selective layer manufacturing and processing) of the hybrid matrix.

Water uptake

Figure 6 shows the absorption of water in the various nanocellulose samples prepared in the study. The measurements were performed at 35°C, and the water uptake is expressed as the total amount of water per sample mass (g_w/g_{pol}) as a function of water activity (p/p^{sat}). MFC-PEG8 and MFC-β-Alanine were excluded from the study as they resulted in unstable dispersions in SHPAA/PVA matrix (discussed in later sections). The water sorption of all other four nanofillers (MFC, CMC, MFC-PPG and MFC-PEG4) exhibited mostly sigmoidal curves

typical of cellulose-based materials. The uptake capacity (0.08 g_w/g_{pol} at 75% RH) of MFC was found to be in agreement with literature[10]. On the other hand, the CMC used in the current study which is derived from Eucalyptus pulp (0.08 g_w/g_{pol} at 47% RH) exhibits higher water sorption than CMC derived from pine and spruce (0.08 g_w/g_{pol} at 70% RH) [40]. As already pointed out in a previous study[10], the raw material used for the MFC fabrication may have significant impact on the mass transport properties.

While all functionalized nanofillers had increased water sorption at higher humidity ranges, it should be noted that the behaviour at high humidity conditions is found to be largely dependent on the functionalized moiety type. While CMC and MFC-PEG4 exhibited an upturn with a steeper slope starting at around 50% RH, the other two variants showed a quite linear increase[41]. The behaviour is attributed to the swelling of the matrix with the formation of water clusters, according to the Park model [12], as an extension of dual-sorption model. Given the polarity of charged moieties and the high hydrophilicity, PEG, CMC and MFC-PEG4 are characterized by excessive swelling, leading to the formation of water clusters formation. Similar results were obtained by Minelli et al. [40] in water sorption studies on MFC plasticized with glycerol. Interestingly, when compared to the MFC, PPG has increased the hydrophilicity of the nanofibrils while delaying the dilation. This delay led to incomplete swelling of the matrix (decreased water uptake [42]) due to the presence of larger alkyl groups when compared to PEG. The uptake of both CMC and MFC-PEG4 was as high as 0.18 g_w/g_{pol} 67% RH and 0.16 g_w/g_{pol} at 65%RH, which translates to an increase of about 140% and 110% increase with respect to unmodified MFC at a similar water activity.

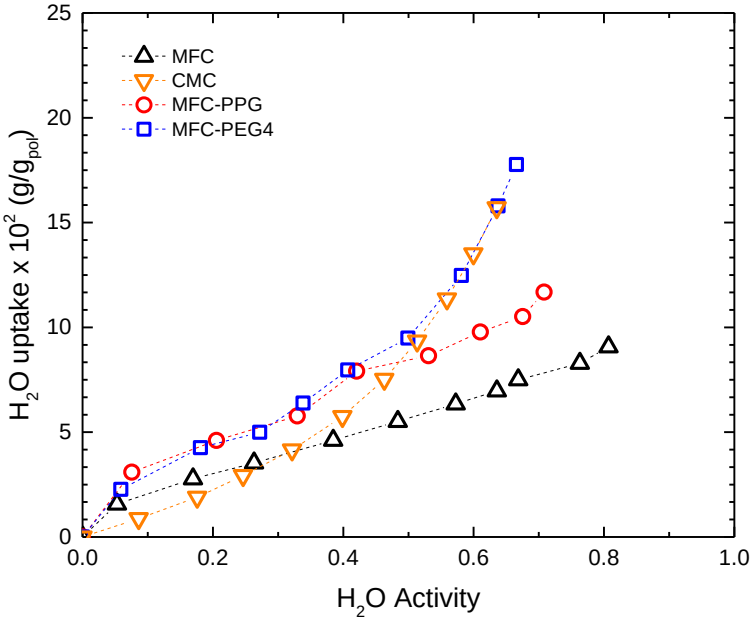

Figure 6. Water uptake capacities of select-modified and unmodified nanofibrils measured at 35 °C. Dashed lines are used to connect the data points for approximate trends.

3.2. Hybrid membranes

Preparation of coating solutions

Two types of membranes were fabricated by incorporating the functionalized nanofillers into two different polymer matrices: the hydrophilic PVA, and the SHPAA blended with 10%PVA containing 40 wt% mobile carrier 2-(1-piperazinyl)ethylamine sarcosinate. The latter is considered to provide facilitated transport effect for CO_2 transport. Physical blending followed by mechanical stirring was used to disperse the nanofillers in the polymer matrices. All functionalized fillers formed homogeneous casting solutions with PVA. Homogeneous dispersions were also observed in the case of the SHPAA/PVA blend, except for MFC-PEG8 and MFC-β-Alanine, which formed visible white aggregates in the SHPAA/PVA blend. When compared to PVA, the environment of SHPAA/PVA can vastly affect the dispersion stability of fillers, partly due to the basic environment and partly due to the presence of amino acid salts that are used as mobile carriers (according to DLVO theory[43]). Functionalization with polymeric moieties tends to increase the steric stabilization while the charged CMCs are stabilized by electrostatic repulsion. Although branched PEGs have been used to increase the dispersion stability of cellulose and various other nanofillers in aqueous solutions[44,45], with the nanofibrils acting as the supports, the 8-arm PEG used in this study tends to form continuous gel network owing to its higher molecular weight. The network is believed to accumulate

together upon the change of environment from an aqueous system to a basic polymer solution containing salt. On the other hand, in the case of β-Alanine, the functionalization leads to decreased charges and lowered acidity of the COOH group of the amino acid. These characteristics play little role in dispersibility in aqueous/PVA solutions, but they decrease the electrostatic interactions in SHPAA/PVA solutions, consequently reducing the overall energy barrier, thus leading to self-aggregation. Surprisingly, MFC had no visible aggregates in macroscopic scale when dispersed in both matrices, which can be attributed to the native charges arising from the hemicellulose content [46].

Fabrication of thin composite membranes

Composite membranes were fabricated from the resulting stable dispersions and were examined in SEM for morphological analysis. Fluorinert™ FC72 was used as pore-filling agent, to avoid pore penetration by the polymer matrix. The compatibility of PVDF with the dispersions led to defect-free coating in large flat sheet membranes (up to 20 x 30 cm). The cross-sectional analysis revealed that the selective layer is approximately 100 – 300 nm thick (Figure 7). It is expected that with increasing nanofiller content in the dispersion, the thickness of the selective layer increases, owing to the increased viscosity and decreased density of the dry solids, which is similar to results from other studies [47]. Composite membranes with such defect-free ultrathin selective layer help in achieving high trans membrane flux to achieve targets of CO_2 separation[9]. Additionally, use of versatile bar coating method for coating also demonstrates potential of scaling up to large area as flat sheet modules [48]. SEM surface images show no clear difference between neat polymer and surfaces of hybrid membranes.

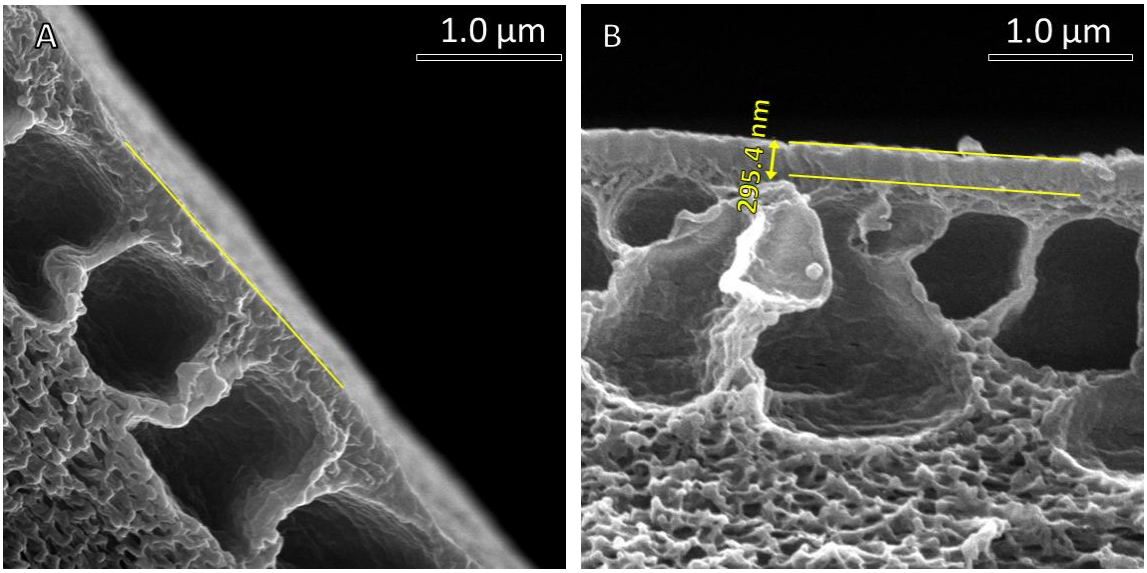

Figure 7. Cross-section SEM images of (A) porous PVDF support (B) Neat SHPAA/PVA composite membrane

AFM

Distribution of fibrils in polymer matrix was studied with AFM imaging for topography and adhesion. Typical entangled network of 1D fibrils were seen in all hybrid surfaces[13,49]. **Figure 8** shows a comparison of AFM height and adhesion images of MFC and MFC-PEG4 dispersed in SHPAA/PVA matrix. The neat polymer matrix of SHPAA/PAA showed a smooth topology with high adhesion. No visible phase separated the polymeric domains, confirming the homogeneity in the blend of SHPAA/PVA in the presence of amino acid salt. The roughness of the hybrid surfaces containing nanocellulose fibrils was considerably higher than the neat polymer surface. Nanoscale aggregates of unmodified MFC were clearly seen in the AFM imaging although no visible aggregates were seen at the dispersion level. The binding of the fibrils at the nano-level due to their poor stability also results in increased self-adhesion which causes the formation of local crystalline phases in the matrix. This binding may also be due to increased H-bonding within the fibrils (inter-fibrillar) leading to formation of bundles because of the increased orderliness at the fibril level. In addition, the highest roughness measured also ascertains possibilities of defects when coated in large areas. By contrast, all modified nanofibrils exhibited random-in-plane swirled orientation and the web-like network is found to coexist synergistically with the polymer matrix surrounding the fibrils, as confirmed by increased adhesion around the fibril edges[50]. This gives evidence of the increased compatibility of the fillers when functionalized with polymer moieties[51]. The functionalized polymer moieties act as bridges which coherently adhere with the polymer matrix upon drying while overcoming the inter-fibrillar hydrogen bonding that leads to compaction of fibres into thick dense fibre bundles. Furthermore, such a web-like dispersion of fibres with retention of individual surfaces gives rise to a more exposed surface area of nanofiller in the hybrid matrix.

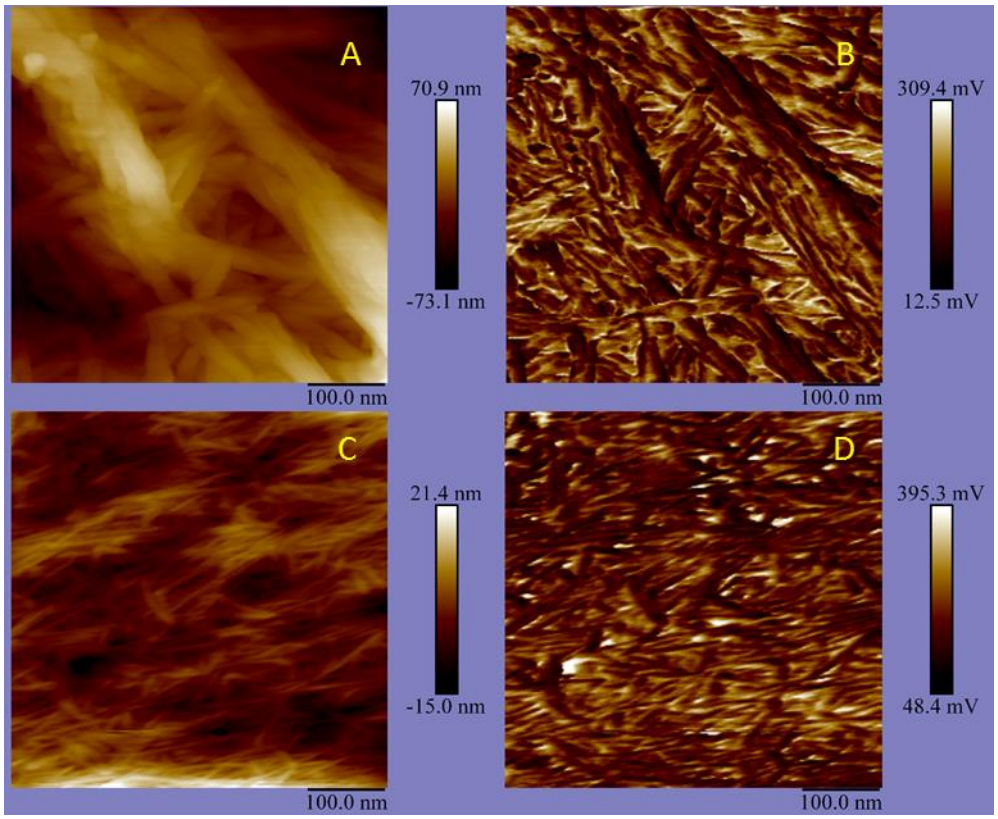

Figure 8. AFM imaging of MFC (A, B) and MFC-PEG4 (C, D) in SHPAA/PVA matrix (A and C are height images; B and D are Adhesion images)

3.3. Permeation properties

Mixed gas permeation tests

The gas permeation tests on the fabricated composite membranes were performed using 90/10 v/v CO_2/N_2 mixture under fully (100% RH) humidified conditions at 35°C. The separation performances of the hybrid membranes based on PVA are shown in **Figure 9**. As can be seen, the membrane of neat PVA exhibits a CO_2 permeance of 240 GPU and a CO_2/N_2 selectivity of 40. The addition of nanocellulose fibrils increased the CO_2 permeance in all cases except for the matrix containing 10% of original nanocellulose, MFC, in which a slight decrease is observed.

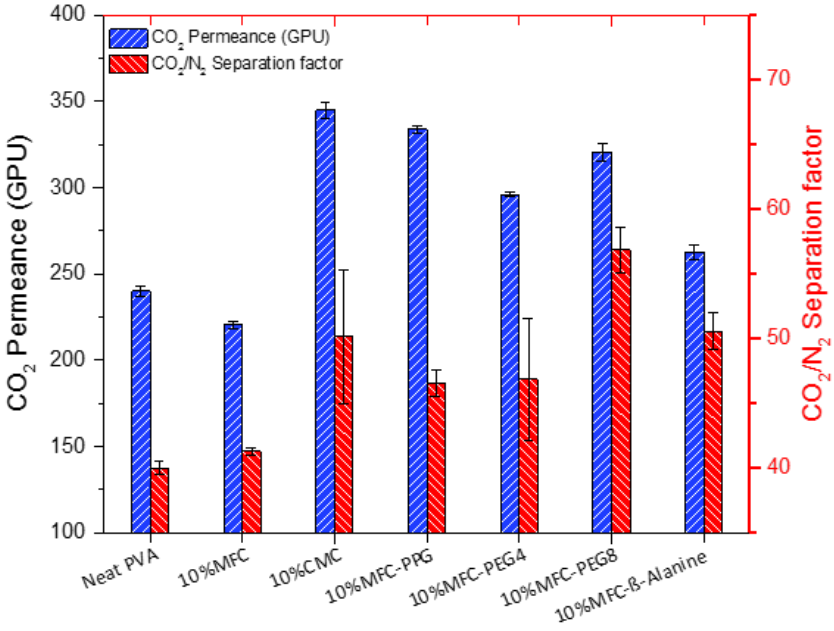

Figure 9. Mixed gas permeation performance of various PVA-based hybrid membranes measured at 35 °C.

Nanocellulose fibrils are renowned for their barrier property in dry conditions or in the low humidity range. However, when nanocellulose fibrils are added to PVA, particularly in low quantities, and under high humidity conditions, their long lateral dimension plays a cogent role in disrupting the H-bonding thereby influencing the local cross-linking of PVA surrounding the fibrils. This disruption of polymer chains surrounding the fibrils bolsters enhanced swelling of the matrix, consequently increasing the diffusion of small molecules[52]. The hydrophilic polymer-filler interface also leads to the retention of water-rich domains around the fibrils. The surface groups in the modified fibrils act as CO_2 transport agents, increasing CO_2 transport in the hybrid matrix. Although the water uptake of PVA is much higher than that of all the studied fibrils [53], the sorption kinetics of nanocellulose fibrils are much faster, leading to faster equilibrium sorption [54,55]. Hence, the faster kinetics can also contribute to easier diffusion of water molecules into the surrounding PVA thereby influencing the gas transport in the hybrid matrix.

Among all the samples, the highest increase was found from the hybrid membrane with 10% CMC, where the CO_2 permeance increased about 43% (345 GPU) with the simultaneous increase in CO_2/N_2 selectivity (from 40 to 50). This improvement may be related to the effect of ionic salt and deprotonated $–COO^-$ groups that become inherently more affinitive to polar CO_2 molecules. The nanofillers functionalized with polymeric moieties displayed positive

effects in increasing both CO_2 permeance and selectivity, but in different extents, possibly related to the different water sorption behaviour (Figure 6), decreased filler phase crystallinity (Table 1), as well as the increased CO_2 affinity resulting from the presence of the EO groups in PEG and PPG functionalities. As a CO_2-philic amino acid, β-Alanine possibly led to increased CO_2 solubility in the hybrid matrix, thus increasing the CO_2 permeance marginally up to 263 GPU and CO_2/N_2 selectivity to 50.

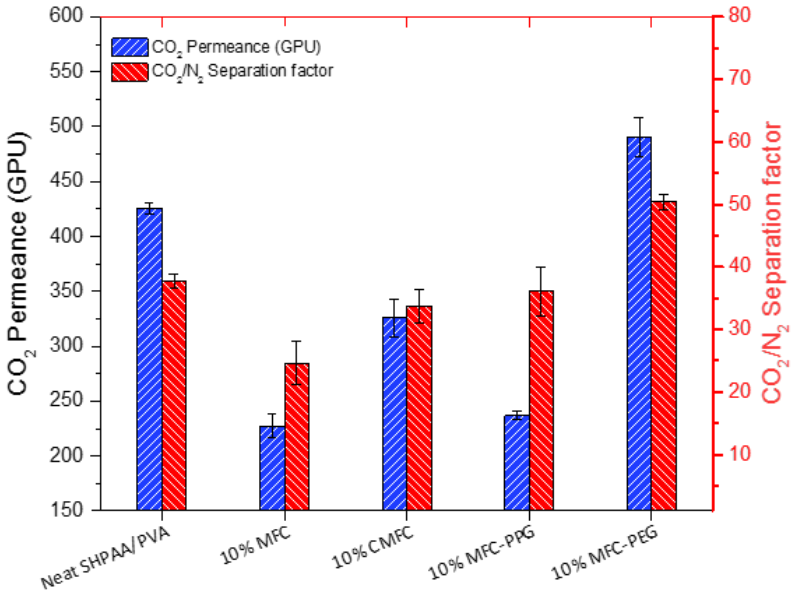

Figure 10. Mixed gas permeation performance of various SHPAA/PVA-based hybrid membranes measured at 35 °C.

Unlike PVA, the functionalized fillers showed unique effects in gas permeation properties when added to a matrix of SHPAA/PVA as shown in **Figure 10**. The membranes containing sterically-hindered PAA and PVA with amino acid mobile carriers showcased CO_2 permeance of 425 GPU and a CO_2/N_2 selectivity of 38. The amine groups present in both the main chain and the mobile carriers contributed to an increase in the CO_2 permeance compared to the neat PVA, due to the facilitated transport mechanism involving the reversible reaction of these amino-groups with CO_2 in presence of water [56,57]. While none of the fillers have such reactive carriers, they help in sorption and retention of water, which is equally an important component in the facilitated transport [25,58] and help to increase the separation performance. Hence, the addition of hydrophilic nanofillers serves a dual purpose of increasing gas permeation due to increased water retention and mechanical reinforcement of the fully swollen polymer matrix at high humidity conditions[25,56,59]. The amine groups, together with the KOH from the synthesis

and purification of the SHPAA polymer, results in a basic polymer solution with a pH close to 12. The fibrils' surface properties play a vital role in the behaviour of nanofillers in basic SHPAA/PVA environment thus influencing the transport properties of the hybrid matrix. Clearly, in the case of MFC, the decreased surface charges led to increased unstable dispersion forming highly crystalline bundles as confirmed with AFM (Figure 7). Both the increased crystallinity and decreased exposed surface due to agglomeration lowered the CO_2 permeance (227 GPU) and CO_2/N_2 selectivity (25).

On the other hand, the functionalized MFCs were well-dispersed in the polymer matrix exploiting the active surface of the nanofillers. In the case of CMC, the charged moieties deprotonate to a larger extent due to the basic amine groups in polymer[60]. While this helps in dispersibility due to electrostatic stabilisation, deprotonation leads to lowered efficiency of amine groups that now stabilize the counter Na^+ ion rather than being involved in the facilitated transport mechanism. Although MFC-PPG had the lowest filler-phase crystallinity, the lower water sorption of MFC-PPG associated with the higher alkyl chain could lead to lower water uptake in the hybrid matrix. Given that the PPG moieties help in dispersion by acting as bridges between the fillers and the polymeric matrix, the interface is still less hydrophilic than that of PEG, thus negatively affecting the CO_2 permeance (237 GPU). Only MFC-PEG showed an increase in both CO_2 permeance and CO_2/N_2 selectivity to about 490.8 GPU and 50.5, respectively. PEGlyation of MFC serves three purposes in the SHPAA-based membrane: firstly, the PEG chains increase the steric stability of the fibrils, as the charges are significantly lower after functionalization; secondly, the EO groups directly contribute to increased surface CO_2 sorption, creating enhanced surface diffusion pathways for CO_2 transport; thirdly, the high hydrophilicity of the PEG chains creates water reservoirs along the surface, enabling swelling of the hybrid matrix and enhancing the facilitated transport effect.

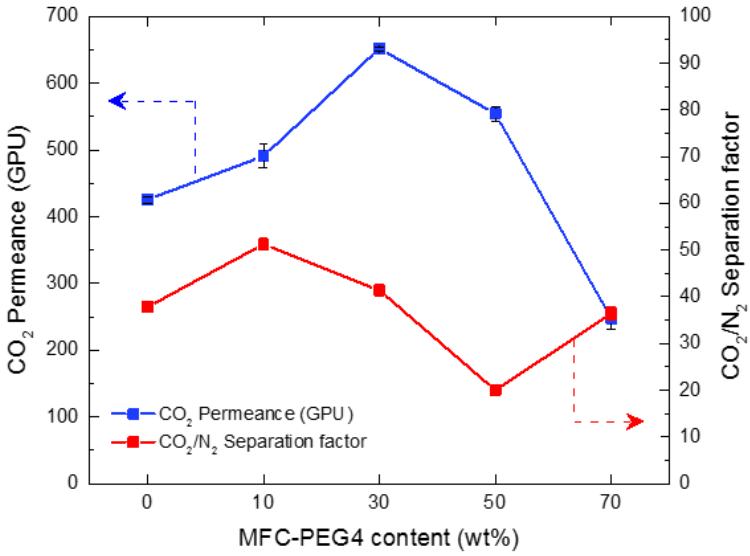

Figure 11. Mixed gas permeation performance of SHPAA/PVA- MFC-PEG4 membranes as a function of filler loading measured at 35 °C

As the most promising filler, MFC-PEG4 was chosen to study the effect of filler loading on permeation properties. The results are presented in **Figure 11**. Increasing the filler loading led to a sharp rise in CO_2 permeance up to 30 wt% (to about 652 GPU), after which a decline in the trend was pronounced. Increase in filler loading leads to an increase in polymer chain disruption, thus enabling higher water retention and availability for gas transport due to decreased polymer crosslinking and increased small molecule diffusion. While the increased loading aids the facilitated transport of CO_2 through the membrane, it should be noted that this is accompanied by a decrease in the number of reactive amine groups. Hence, it is expected that there exists an optimum loading where the local environmental changes triggered by the fibrils are just enough for effective utilization of the reactive amines present in the polymer matrix and the mobile carriers. Below this optimum, the reactive carriers are under-exploited, and the lower availability of water and increased amount of crystalline polymer phase would lead to decreased selectivity.

The overall swelling of polymer matrix is reduced due to the increased reinforcement of the hybrid matrix caused by fibre entanglement. This effect leads to domains of the dense fibre network and sparse fibres in water-rich regions that decrease the selectivity. The dense regions also inherit the barrier property of nanocellulose fibrils thus lowering the permeance. At the concentration of around 50% MFC-PEG, the dispersion was stable only for a short time, which may be attributed to the critical transition concentration where the dispersion changes from polymer-rich solution to MFC-rich solution. On the other hand, increased loading of nanofibers

may result in increased local defects in the membrane due to the lower density and higher viscosity of the nanocellulose phase.

Additionally, it has to be noted that the nanocellulose fibrils tend to increase the selective layer thickness due to increased viscosity and low density**.** Since the permeance is dependent on the selective layer thickness, the lower permeance at the loading of 70 wt% may also be related to a thicker selective layer. However, it is not feasible to coat membranes of the same thickness with different ratios of polymers and nanocellulose; for membranes with a higher nanocellulose loading, lowering concentration in cast solution in order to reduce the thickness may cause defects in the selective layer.

Although several studies have been reported using nanocellulose as fillers in hybrid matrices, most performance evaluation of the materials has been as self-standing films. There exists few studies with nanocellulose fibrils-based hybrid membranes in the form of thin film composite membranes. Dai et al. [47] reported a maximum permeance of 470.8 GPU with a CO_2/N_2 selectivity of 34.6 as hollow fiber membranes with 80 % MFC in PVA matrix. In another study as flat-sheet membrane, Torstensen et al. [61] reported a performance of 100 GPU with a CO_2/N_2 selectivity of 42 using phosphorylated nanocellulose fibrils as fillers in PVA matrix. The fabricated membrane with 30 wt% MFC-PEG4 with a CO_2 permeance of 652 and CO_2/N_2 selectivity of 41.3 surpasses performance of all reported hybrid membranes that use MFC in the form of composites.

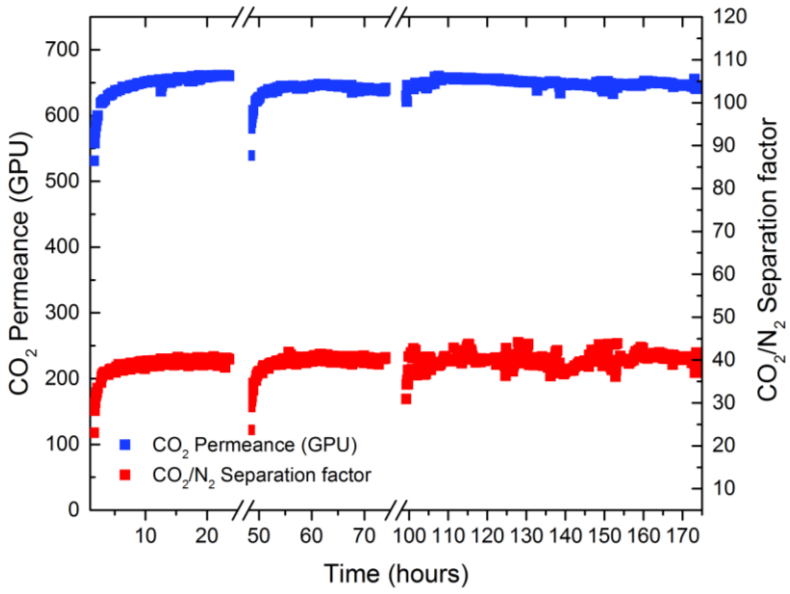

Figure 12. Permeation stability tests with forced breaks of SHPAA/PVA- 30 wt% MFC- PEG4 membranes measured at 35 °C

In order to demonstrate the stability of the fabricated hybrid membrane, SHPAA/PVA hybrid with 30 wt% loading of MFC-PEG4 filler was subjected to humid mixed gas permeation tests for an extended period of about 175 h. Stable performances were recorded throughout the period with minimal changes to both CO_2 permeance and CO_2/N_2 selectivity as seen in Figure 12. Humidity fluctuations play a major role in the performance of facilitated transport membranes as small changes in RH conditions of the feed stream leads to significant drop in fluxes[62,63]. As the addition of nanocellulose helps in water retention, the superstructure of the hybrid matrix is expected to be less prone to changes due to exposed humidity fluctuations. In order to demonstrate this phenomenon, two forced breaks of 24 h each were introduced where the membrane was stored in room temperature conditions. It can be clearly seen that the performance of the fabricated membranes is recoverable after such breaks, which can be considered analogous to disruptions in feed gas conditions. Similar long-term stability of nanocellulose-based hybrid membrane has also been reported in our previus work[47].

4. Conclusions

A rapid one-pot functionalization procedure was used to successfully modify the surface of nanacellulose fibrils additives in membranes for enhanced CO_2 separation. The modification led to profound changes in specific properties of the nanofibers, like crystallinity, water uptake and thermal stability. The functional groups attached to the surface acted as manipulative tools to control interface properties in favour of application in CO_2 transport membranes, depending on their characteristics.

Hybrid composite membranes containing both modified and unmodified fibrils with two different polymer matrices (PVA and SHPAA/PVA blend) was successfully fabricated and tested. Functionalization of fibrils surfaces was found to play a crucial role in dispersibility of fibrils in facilitated transport polymers like SHPAA. All functionalized moieties were found to act as a bridge to form a compatible interface between cellulosic surface and the main polymer matrix, thus preventing self-aggregation of these fillers. The CO_2 transport properties in the hybrid matrices were largely dependent on the dispersibility and interface properties of the nanocellulose, which was manipulated with the type of functional moieties used in this work. A correlation between the tuned surfaces and the transport properties was clearly established. At 30 wt% loading, MFC-PEG4 showed the most profound influence on the separation

performance of the facilitated transport membranes by increasing the CO_2 permeance to about 50% (up to 652 GPU) while retaining the selectivity of the neat polymer matrix. The membrane was also found to be stable over long-term period of 175 h with fluctuations in operating conditions. While standalone nanocellulose exhibits barrier property, the synergetic interaction of these bio-nanofillers with facilitated transport resulted in hybrid materials with interesting separation performances. The importance of surface properties of nanofillers in hybrid materials for gas separation has been successfully demonstrated. This foreruns potential studies on tuning of nanofillers for applications in various hybrid gas separation membranes.

Conflicts of Interest

The authors declare no conflicts of interest.

Acknowledgements

The Research Council of Norway is acknowledged for the support to the Norwegian Micro- and Nano-Fabrication Facility, NorFab, project number 245963/F50. The authors thank Torun Margareta Melø for help with the NMR measurements.

Author Contributions

S.J., L.A. and Z.D. designed the experiments. X.Y. and S.J. synthesized the nanofillers. X.Y. performed S(T)EM, TGA, FTIR, XRD and conducted some permeation tests (PVA). S.J. performed other tests, analysed the results, and wrote the manuscript. L.D. and L.A. conceived the idea, the overall study and supervised the research work.

Associated Content

Supporting Information available: Surface SEM images of fabricated membranes

References

(1) Beecher, J. F., Organic Materials: Wood, Trees and Nanotechnology, *Nat. Nanotechnol.* **2007**, pp 466–467.
(2) Habibi, Y.; Lucia, L. A.; Rojas, O. J., Cellulose Nanocrystals: Chemistry, Self-Assembly, and Applications, *Chem. Rev.* **2010**, *110* (6), 3479–3500.
(3) Zhang, S.; Sun, G.; He, Y.; Fu, R.; Gu, Y.; Chen, S., Preparation, Characterization, and

Electrochromic Properties of Nanocellulose-Based Polyaniline Nanocomposite Films, *ACS Appl. Mater. Interfaces* **2017**, *9* (19), 16426–16434.
(4) Dufresne, A., Nanocellulose: A New Ageless Bionanomaterial, *Mater. Today* **2013**, *16* (6), 220–227.
(5) Abitbol, T.; Rivkin, A.; Cao, Y.; Nevo, Y.; Abraham, E.; Ben-Shalom, T.; Lapidot, S.; Shoseyov, O., Nanocellulose, a Tiny Fiber with Huge Applications, *Curr. Opin. Biotechnol.* **2016**, *39* (I), 76–88.
(6) Soeta, H.; Fujisawa, S.; Saito, T.; Berglund, L.; Isogai, A., Low-Birefringent and Highly Tough Nanocellulose-Reinforced Cellulose Triacetate, *ACS Appl. Mater. Interfaces* **2015**, *7* (20), 11041–11046.
(7) Yang, X.; Berthold, F.; Berglund, L. A., High-Density Molded Cellulose Fibers and Transparent Biocomposites Based on Oriented Holocellulose, *ACS Appl. Mater. Interfaces* **2019**, *11* (10), 10310–10319.
(8) Janakiram, S.; Ahmadi, M.; Dai, Z.; Ansaloni, L.; Deng, L., Performance of Nanocomposite Membranes Containing 0D to 2D Nanofillers for CO_2 separation: A Review, *Membranes*. **2018**, *8*, 24–59.
(9) Park, H. B.; Kamcev, J.; Robeson, L. M.; Elimelech, M.; Freeman, B. D., Maximizing the Right Stuff: The Trade-off between Membrane Permeability and Selectivity, *Science.* **2017**, *356*, eaab0530.
(10) Ansaloni, L.; Salas-Gay, J.; Ligi, S.; Baschetti, M. G., Nanocellulose-Based Membranes for CO_2 Capture, *J. Memb. Sci.* **2017**, *522*, 216–225.
(11) Venturi, D.; Grupkovic, D.; Baschetti, M. G.; Sisti, L., Effect of Humidity and Nanocellulose Content on Polyvinylamine-Nanocellulose Hybrid Membranes for CO_2 Capture, *J. Memb. Sci.* **2017**, 548, 263–274.
(12) Park, G. S., Transport Principles—Solution, Diffusion and Permeation in Polymer Membranes, *Synthetic Membranes: Science, Engineering and Applications*; 1986; pp 57–107.
(13) Klemm, D.; Kramer, F.; Moritz, S.; Lindström, T.; Ankerfors, M.; Gray, D.; Dorris, A., Nanocelluloses: A New Family of Nature-Based Materials, *Angew. Chemie - Int. Ed.* **2011**, *50* (24), 5438–5466.
(14) Voisin, H.; Bergström, L.; Liu, P.; Mathew, A., Nanocellulose-Based Materials for Water Purification, *Nanomaterials* **2017**, *7* (3), 57.
(15) Karim, Z.; Claudpierre, S.; Grahn, M.; Oksman, K.; Mathew, A. P., Nanocellulose Based Functional Membranes for Water Cleaning: Tailoring of Mechanical Properties, Porosity and Metal Ion Capture, *J. Memb. Sci.* **2016**, *514*, 418–428.
(16) Dai, Z.; Ansaloni, L.; Deng, L., Recent Advances in Multi-Layer Composite Polymeric Membranes for CO_2 Separation: A Review, *Green Energy Environ.* **2016**, *1*(2), 102–128
(17) Ansaloni, L.; Deng, L., Advances in Polymer-Inorganic Hybrids as Membrane Materials, *Recent Developments in Polymer Macro, Micro and Nano Blends* **2016**, *7*, 163.
(18) Kalia, S.; Dufresne, A.; Cherian, B. M.; Kaith, B. S.; Avérous, L.; Njuguna, J.; Nassiopoulos, E., Cellulose-Based Bio- and Nanocomposites: A Review, *International Journal of Polymer Science*. **2011**., Article ID 837875
(19) Jorfi, M.; Foster, E. J., Recent Advances in Nanocellulose for Biomedical Applications, *J. Appl. Polym. Sci.* **2015**, *132* (14), 1–19.
(20) Díez, I.; Eronen, P.; Österberg, M.; Linder, M. B.; Ikkala, O.; Ras, R. H., Functionalization of Nanofibrillated Cellulose with Silver Nanoclusters: Fluorescence and Antibacterial Activity, *Macromol. Biosci.* **2011**, *11* (9), 1185–1191.
(21) Jin, L.; Li, W.; Xu, Q.; Sun, Q., Amino-Functionalized Nanocrystalline Cellulose as an

Adsorbent for Anionic Dyes, *Cellulose* **2015**, *22* (4), 2443–2456.
(22) Ahmadi, M.; Janakiram, S.; Dai, Z.; Ansaloni, L.; Deng, L., Performance of Mixed Matrix Membranes Containing Porous Two-Dimensional (2D) and Three-Dimensional (3D) Fillers for CO_2 separation: A Review, *Membranes*. **2018**, *8*, 1–48.
(23) Shen, Y.; Wang, H.; Liu, J.; Zhang, Y., Enhanced Performance of a Novel Polyvinyl Amine/Chitosan/Graphene Oxide Mixed Matrix Membrane for CO_2 Capture, *ACS Sustain. Chem. Eng.* **2015**, *3* (8), 1819–1829.
(24) Li, X.; Cheng, Y.; Zhang, H.; Wang, S.; Jiang, Z.; Guo, R.; Wu, H., Efficient CO_2 Capture by Functionalized Graphene Oxide Nanosheets as Fillers to Fabricate Multi-Permselective Mixed Matrix Membranes, *ACS Appl. Mater. Interfaces* **2015**, *7* (9), 5528–5537.
(25) Ansaloni, L.; Zhao, Y.; Jung, B. T.; Ramasubramanian, K.; Baschetti, M. G.; Ho, W. S. W., Facilitated Transport Membranes Containing Amino-Functionalized Multi-Walled Carbon Nanotubes for High-Pressure CO_2 Separations, *J. Memb. Sci.* **2015**, *490*, 18–28.
(26) Zhao, Y.; Ho, W. S. W., Steric Hindrance Effect on Amine Demonstrated in Solid Polymer Membranes for CO_2 Transport, *J. Memb. Sci.* **2012**, *415–416*, 132–138.
(27) Ansaloni, L.; Rennemo, R.; Knuutila, H. K.; Deng, L., Development of Membrane Contactors Using Volatile Amine-Based Absorbents for CO_2 Capture : Amine Permeation through the Membrane, *J. Memb. Sci.* **2017**, *537*, 272–282.
(28) Minelli, M.; Cocchi, G.; Ansaloni, L.; Baschetti, M. G.; De Angelis, M. G.; Doghieri, F., Vapor and Liquid Sorption in Matrimid Polyimide: Experimental Characterization and Modeling, *Ind. Eng. Chem. Res.* **2013**, *52* (26), 8936–8945.
(29) Chiara Ferrari, M.; Galizia, M.; De Angelis, M. G.; Cesare Sarti, G., Vapor Sorption and Diffusion in Mixed Matrices Based on Teflon® AF 2400, *Membrane Gas Separation*. August 13, 2010.
(30) Dai, Z.; Ansaloni, L.; Ryan, J. J.; Spontak, R. J.; Deng, L., Nafion/IL Hybrid Membranes with Tuned Nanostructure for Enhanced CO_2 separation: Effects of Ionic Liquid and Water Vapor, *Green Chem.* **2018**, *20* (6), 1391–1404.
(31) Eyholzer, C.; Bordeanu, N.; Lopez-Suevos, F.; Rentsch, D.; Zimmermann, T.; Oksman, K., Preparation and Characterization of Water-Redispersible Nanofibrillated Cellulose in Powder Form, *Cellulose* **2010**, *17* (1), 19–30.
(32) Lak, A.; Dieckhoff, J.; Ludwig, F.; Scholtyssek, J. M.; Goldmann, O.; Lünsdorf, H.; Eberbeck, D.; Kornowski, A.; Kraken, M.; Litterst, F. J.; Fiege, K.; Mischnick, P.; Schilling, M., Highly Stable Monodisperse PEGylated Iron Oxide Nanoparticle Aqueous Suspensions: A Nontoxic Tracer for Homogeneous Magnetic Bioassays, *Nanoscale* **2013**, *5* (23), 11447–11455.
(33) Pääkko, M.; Ankerfors, M.; Kosonen, H.; Nykänen, A.; Ahola, S.; Österberg, M.; Ruokolainen, J.; Laine, J.; Larsson, P. T.; Ikkala, O.; Lindström, T., Enzymatic Hydrolysis Combined with Mechanical Shearing and High-Pressure Homogenization for Nanoscale Cellulose Fibrils and Strong Gels, *Biomacromolecules* **2007,** *8* (6), 1934–1941.
(34) Onyianta, A. J.; Dorris, M.; Williams, R. L., Aqueous Morpholine Pre-Treatment in Cellulose Nanofibril (CNF) Production : Comparison with Carboxymethylation and TEMPO Oxidisation Pre-Treatment Methods, *Cellulose* **2018**, *25* (2), 1047–1064.
(35) Segal, L.; Creely, J. J.; Martin Jr., A. E.; Conrad, C. M., Empirical Method for Estimating the Degree of Crystallinity of Native Cellulose Using the X-Ray Diffractometer, *Text. Res. J.* **1959**, 786–794.
(36) Biswal, D. R.; Singh, R. P., Characterisation of Carboxymethyl Cellulose and Polyacrylamide Graft Copolymer, *Carbohydr. Polym.* **2004**, *57* (4), 379–387.

(37) Zhou, S.; Dong, J.; Lu, C.; Li, B.; Li, F.; Zhang, B.; Wang, H.; Wei, Y., Effect of Sodium Carbonate on Phase Transformation of High-Magnesium Laterite Ore, *Mater. Trans.* **2017**, *58* (5).
(38) Ochoa, M.; Collazos, N.; Le, T.; Subramaniam, R.; Sanders, M.; Singh, R. P.; Depan, D., Nanocellulose-PE-b-PEG Copolymer Nanohybrid Shish-Kebab Structure via Interfacial Crystallization, *Carbohydr. Polym.* **2017**, *159*, 116–124.
(39) Lin, H.; Kai, T.; Freeman, B. D.; Kalakkunnath, S.; Kalika, D. S., The Effect of Cross-Linking on Gas Permeability in Cross-Linked Poly(Ethylene Glycol Diacrylate), *Macromolecules* **2005**, *38* (20), 8381–8393.
(40) Minelli, M.; Baschetti, M. G.; Doghieri, F.; Ankerfors, M.; Lindström, T.; Siró, I.; Plackett, D., Investigation of Mass Transport Properties of Microfibrillated Cellulose (MFC) Films, *J. Memb. Sci.* **2010**, *358* (1–2), 67–75.
(41) Meriçer, Ç.; Minelli, M.; Baschetti, M. G., Water Sorption in Microfibrillated Cellulose (MFC): The Effect of Temperature and Pretreatment, **2017**, *174*, 1201–1212.
(42) Amick, R.; Gilbert, R. D.; Stannett, V., Preparation and Water Sorption Properties of Cellulose-Polypropylene Glycol Block Copolymers, *Polymer (Guildf).* **1980**, *21* (6), 648–650.
(43) Bizmark, N.; Ioannidis, M. A., Effects of Ionic Strength on the Colloidal Stability and Interfacial Assembly of Hydrophobic Ethyl Cellulose Nanoparticles, *Langmuir* **2015**, *31* (34), 9282–9289.
(44) Prencipe, G.; Tabakman, S. M.; Welsher, K.; Liu, Z.; Goodwin, A. P.; Zhang, L.; Henry, J.; Dai, H., PEG Branched Polymer for Functionalization of Nanomaterials with Ultralong Blood Circulation, *J. Am. Chem. Soc.* **2009**, *131* (13), 4783–4787.
(45) Hutanu, D., Recent Applications of Polyethylene Glycols (PEGs) and PEG Derivatives. *Mod. Chem. Appl.* **2014**, *02* (02).
(46) Fall, A. B.; Lindström, S. B.; Sundman, O.; Odberg, L.; Wagberg, L., Colloidal Stability of Aqueous Nanofibrillated Cellulose Dispersions, *Langmuir* **2011**, *27* (18), 11332–11338.
(47) Dai, Z.; Deng, J.; Yu, Q.; Helberg, R. M. L.; Janakiram, S.; Ansaloni, L.; Deng, L., Fabrication and Evaluation of Bio-Based Nanocomposite TFC Hollow Fiber Membranes for Enhanced CO_2 Capture, *ACS Appl. Mater. Interfaces* **2019**, *11*, 10874–10882.
(48) Yoo, M. J.; Lee, J. H.; Yoo, S. Y.; Oh, J. Y.; Roh, J. M.; Grasso, G.; Lee, J. H.; Lee, D.; Oh, W. J.; Yeo, J. gu; Cho, Y. H.; Park, H. B., Defect Control for Large-Scale Thin-Film Composite Membrane and Its Bench-Scale Demonstration, *J. Memb. Sci.* **2018**, *566*, 374–382.
(49) Luong, N. D.; Korhonen, J. T.; Soininen, A. J.; Ruokolainen, J.; Johansson, L. S.; Seppälä, J., Processable Polyaniline Suspensions through in Situ Polymerization onto Nanocellulose, *Eur. Polym. J.* **2013**, *49* (2), 335–344.
(50) Salajkova, M.; Valentini, L.; Zhou, Q.; Berglund, L. A., Tough Nanopaper Structures Based on Cellulose Nanofibers and Carbon Nanotubes, *Compos. Sci. Technol.* **2013**, *87*, 103–110.
(51) Salas, C.; Nypelö, T.; Rodriguez-Abreu, C.; Carrillo, C.; Rojas, O. J., Nanocellulose Properties and Applications in Colloids and Interfaces, *Curr. Opin. Colloid Interface Sci.* **2014**, *19* (5), 383–396.
(52) Torstensen, J.; Liu, M.; Jin, S. A.; Deng, L.; Hawari, A. I.; Syverud, K.; Spontak, R. J.; Gregersen, Y. W., Swelling and Free-Volume Characteristics of TEMPO-Oxidized Cellulose Nanofibril Films, *Biomacromolecules* **2018**, *19* (3), 1016–1025.
(53) Guo, X.; Wu, Y.; Xie, X., Water Vapor Sorption Properties of Cellulose Nanocrystals

and Nanofibers Using Dynamic Vapor Sorption Apparatus, *Sci. Rep.* **2017**, *7* (1).
(54) Saeed, M.; Deng, L., Carbon Nanotube Enhanced PVA-Mimic Enzyme Membrane for Post-Combustion CO_2 Capture, *Int. J. Greenh. Gas Control* **2016**, *53*, 254–262.
(55) Belbekhouche, S.; Bras, J.; Siqueira, G.; Chappey, C.; Lebrun, L.; Khelifi, B.; Marais, S.; Dufresne, A., Water Sorption Behavior and Gas Barrier Properties of Cellulose Whiskers and Microfibrils Films, *Carbohydr. Polym.* **2011**, *83* (4), 1740–1748.
(56) Deng, L.; Kim, T. J.; Hägg, M. B., Facilitated Transport of CO_2 in Novel PVAm/PVA Blend Membrane, *J. Memb. Sci.* **2009**, *340* (1–2), 154–163.
(57) Zhao, Y.; Ho, W. S. W., CO_2-Selective Membranes Containing Sterically Hindered Amines for CO_2/H_2 Separation. *Ind. Eng. Chem. Res.* **2013**, *52* (26), 8774–8782.
(58) Deng, L.; Hagg, M. B., Carbon Nanotube Reinforced PVAm/PVA Blend FSC Nanocomposite Membrane for CO_2/CH_4 Separation, *Int. J. Greenh. Gas Control* **2014**, *26*, 127–134.
(59) Kim, S.; Chen, L.; Johnson, J. K.; Marand, E., Polysulfone and Functionalized Carbon Nanotube Mixed Matrix Membranes for Gas Separation: Theory and Experiment, *J. Memb. Sci.* **2007**, *294* (1–2), 147–158.
(60) Olszewska, A.; Junka, K.; Nordgren, N.; Laine, J.; Rutland, M. W.; Österberg, M., Non-Ionic Assembly of Nanofibrillated Cellulose and Polyethylene Glycol Grafted Carboxymethyl Cellulose and the Effect of Aqueous Lubrication in Nanocomposite Formation, *Soft Matter* **2013**, *9* (31), 7448–7457.
(61) Torstensen, J.; Helberg, R. M. L.; Deng, L.; Gregersen, Ø. W.; Syverud, K., PVA/Nanocellulose Nanocomposite Membranes for CO_2 Separation from Flue Gas, *Int. J. Greenh. Gas Control* **2019**, *81*, 93–102.
(62) Deng, L.; Hägg, M. B., Techno-Economic Evaluation of Biogas Upgrading Process Using CO_2 Facilitated Transport Membrane, *Int. J. Greenh. Gas Control* **2010**, *4* (4), 638–646.
(63) Hägg, M. B.; Lindbråthen, A.; He, X.; Nodeland, S. G.; Cantero, T., Pilot Demonstration-Reporting on CO_2 Capture from a Cement Plant Using Hollow Fiber Process, *Energy Procedia* **2017**, *114* (1876), 6150–6165.

Graphic Abstract